

Article

Sound Velocity in a Thin Shallowly Submerged Terrestrial-Marine Quaternary Succession (Northern Adriatic Sea)

Ana Novak ^{1,2,*} , Andrej Šmuc ² , Sašo Poglajen ³, Bogomir Celarc ¹ and Marko Vrabec ²

¹ Geological Survey of Slovenia, Dimičeva ulica 14, 1000 Ljubljana, Slovenia; bogomir.celarc@geo-zs.si

² Department of Geology, University of Ljubljana, Faculty of Natural Sciences and Engineering, Aškerčeva 12, 1000 Ljubljana, Slovenia; andrej.smuc@geo.ntf.uni-lj.si (A.Š.); marko.vrabec@geo.ntf.uni-lj.si (M.V.)

³ Sirio d.o.o., Kvedrova cesta 16, 6000 Koper, Slovenia; poglaj@gmail.com

* Correspondence: ana.novak@geo-zs.si; Tel.: +386-128-09-779

Received: 30 December 2019; Accepted: 15 February 2020; Published: 18 February 2020



Abstract: Estimating sound velocity in seabed sediment of shallow near-shore areas submerged after the Last Glacial Maximum is often difficult due to the heterogeneous sedimentary composition resulting from sea-level changes affecting the sedimentary environments. The complex sedimentary architecture and heterogeneity greatly impact lateral and horizontal velocity variations. Existing sound velocity studies are mainly focused on the surficial parts of the seabed sediments, whereas the deeper and often more heterogeneous sections are usually neglected. We present an example of a submerged alluvial plain in the northern Adriatic where we were able to investigate the entire Quaternary sedimentary succession from the seafloor down to the sediment base on the bedrock. We used an extensive dataset of vintage borehole litho-sedimentological descriptions covering the entire thickness of the Quaternary sedimentary succession. We correlated the dataset with sub-bottom sonar profiles in order to determine the average sound velocities through various sediment types. The sound velocities of clay-dominated successions average around 1530 m/s, while the values of silt-dominated successions extend between 1550 and 1590 m/s. The maximum sound velocity of approximately 1730 m/s was determined at a location containing sandy sediment, while the minimum sound velocity of approximately 1250 m/s was calculated for gas-charged sediments. We show that, in shallow areas with thin Quaternary successions, the main factor influencing average sound velocity is the predominant sediment type (i.e. grain size), whereas the overburden influence is negligible. Where present in the sedimentary column, gas substantially reduces sound velocity. Our work provides a reference for sound velocities in submerged, thin (less than 20 m thick), terrestrial-marine Quaternary successions located in shallow (a few tens of meters deep) near-shore settings, which represent a large part of the present-day coastal environments.

Keywords: sound velocity; Quaternary sediment; submerged alluvial plain

1. Introduction

In geophysical (acoustic/seismic) investigations of the subsurface, velocity modeling is essential for converting two-way travel time of the observed reflections into the depth domain. Velocity data are routinely extracted from multi-channel seismic data [1]; however, in many circumstances, particularly in shallow near-shore settings, obtaining offshore multi-channel data is not feasible. Restricted navigation, legal constraints, busy marine traffic, relatively low resolution of the acquired data and the surveying cost itself often make acquisition and maneuvering with streamers and seismic sources impractical or even impossible. In such settings, high-resolution single-channel seismic and acoustic surveys provide a common alternative, but the velocity data must then be obtained by other means, such as in situ

measurements, laboratory core logging, and geo-acoustic modeling [2–20]. Due to costly offshore core drilling, these approaches are mostly focused on the upper few meters of the seafloor sediment. Consequently, the acoustic properties of surficial seafloor sediments have been well known for some time [4,5,11,15,19], but sound velocity in thicker (more than 10 m) sedimentary sequences has rarely been investigated (e.g., [17]). Therefore, when velocity data for depth conversion of single-channel seismic or acoustic data are not acquired during surveying, a velocity value corresponding to the surficial sediment grain size (e.g., [19]) or a previously published value from a nearby location is usually used. Whereas this approach is sufficient for geophysical surveys of uniform sedimentary layers, it produces significant uncertainties when dealing with pronounced lateral and vertical variability in sediment composition and architecture.

Typical example of such complex settings are shallow continental shelf areas drowned during the global sea-level rise that followed the Last Glacial Maximum (LGM) lowstand when the global mean sea level was approximately at -130 m [21,22]. During transgression, earlier terrestrial depositional environments (e.g., alluvial plains) were overlain by terrestrial and marine-derived sediments deposited in fluvial, estuarine, and open marine settings, resulting in complex sedimentary architecture and highly variable sedimentary types [22–24], which markedly affect the sub-bottom propagation of acoustic waves [1]. Precise mapping of the 2D and 3D geometries of the sedimentary bodies in these near-shore shallow environments and their appropriate time-to-depth conversion are essential for reliable interpretation of high-resolution acoustic and seismic surveys, not only for unraveling their depth and depositional history, but also for geotechnical site assessments in various engineering projects.

During the LGM lowstand, vast areas of the presently submerged continental shelves were exposed (e.g., Figure 1a) and amounted to approximately 40% of additional landmass in Europe and 5% globally [25,26]. Therefore, the shallow-most near-shore parts of presently submerged continental shelves extend over a considerable area globally and represent an important and often poorly studied geological environment. Due to the steadily increasing interest of the geological and archaeological research communities in shallow, presently submerged, and often buried landscapes [27–41], accurate depth conversion is crucial for future geological studies and paleoenvironmental reconstructions in such settings. We investigate an example of a transgressed and submerged alluvial plain in the Bay of Koper (Gulf of Trieste, northern Adriatic Sea; Figure 1) to provide sound velocity values for thin (up to 20 m thick) Quaternary sediments deposited in terrestrial-marine sedimentary environments located in shallow near-shore environments a few tens of meters deep. Our work ranks among the few studies that are not limited only to the surficial seafloor sediments, but also include the entire sedimentary succession from the seafloor to the base of the sediment on the bedrock.

Setting

The post-LGM sea-level rise induced significant changes in the sedimentary environments of the northern Adriatic Sea with terrestrial environments transitioning in paralic and later shallow marine environments [22,42–56]. In the Gulf of Trieste, where our study area is located (Figure 1), the Late Pleistocene alluvial plain transitioned into a paralic environment until open marine conditions finally prevailed approximately 10,000 years ago [22,42,44,45,55–64].

The Bay of Koper is located in the southeastern part of the Gulf of Trieste, which represents the northeasternmost extension of the Adriatic Sea (Figure 1). The seabed morphology of the Bay is smooth with depths ranging up to 20 m in the open part (Figure 1b). The main fluvial source draining into the Bay is the Rižana river with its mouth located in the reclaimed eastern part of the Bay within the Port of Koper complex. The smaller Badaševica stream is located west of the city of Koper.

The hinterland of the Bay of Koper is composed of Eocene turbidites (flysch) comprising interbedded sandstones and marlstones, which are overlain by Quaternary alluvial and paralic sediments in the valleys of Rižana and Badaševica (Figure 1b; [65,66]). Offshore the Eocene succession is unconformably overlain by Quaternary terrestrial and paralic sediments topped by Holocene marine sediments [55,56,59,62,67–71]. The Quaternary succession in the Bay of Koper, which was recognized

as a submerged fluvial valley of the Rižana river (Figure 1b, [68–71]), is up to a few tens of meters thick and is composed of a lower alluvial part and an upper paralic part; however, alternations of terrestrial and paralic sedimentary environments have also been observed [68,72]. The alluvial sediments are generally composed of fine-grained clastic sediments with occasional gravelly and sandy horizons, whereas the paralic sediments are mostly composed of silty clay [68–70]. The Holocene marine cover comprises fine-grained bioclastic sediment with the surficial sediments showing a clear zonation: sandy silt near the coastline, clayey silt in the central part, and silt in the outer part of the Bay [62,68–71]. Holocene sedimentation rates in the Gulf of Trieste are relatively low and amount to a few millimeters per year [44,57,69,73]. Repeated multibeam bathymetric surveys in the Bay of Koper do not show significant changes in the seafloor morphology [74] and therefore imply a low-energy sedimentary environment.

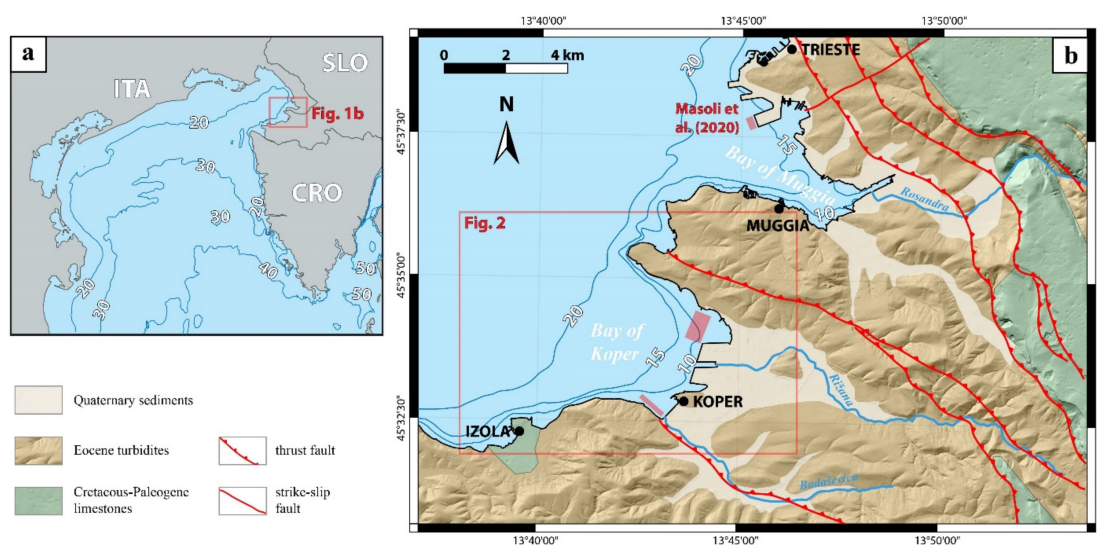


Figure 1. Geographical location of the study area. (a) Regional map of the northern Adriatic, which was entirely subaerially exposed during the Last Glacial Maximum (LGM). Bathymetry data from [75]. (b) Geological map of the hinterland of the Bay of Koper. Two red rectangles in the Bay of Koper mark the areas investigated in this study. The red rectangle in the Bay of Muggia marks the study area of [76]. Bathymetric data are simplified after [77] and [78]. Geological data are simplified after [65,66,79–82].

2. Materials and Methods

We used archive geotechnical reports from the borehole database of the Geological Survey of Slovenia. Boreholes were mainly located in the NE part of the Bay (Figure 2) and were drilled in the late 1980s and early 1990s for geotechnical investigations supporting various infrastructure projects of the Port of Koper. Borehole metadata and descriptions are provided in Table 1 and Figure 5. The boreholes were drilled with rotary drilling and were cored. Sediment core samples were used for geomechanical testing and were not preserved. We therefore reconstructed the borehole sedimentary logs (Figure 5) from borehole descriptions contained in the geotechnical reports.

Sub-bottom sonar profiles were acquired in June 2016 on board vessel Lyra with the Innomar SES-2000 Compact sub-bottom sonar. Profile transects were designed to directly cross the borehole locations. Navigation north of the second pier was obstructed by a containment boom and very shallow water depths near the coastline. For this reason, some of the sub-bottom profiles are located at some distance from the borehole locations (Table 1 and Figure 2b). We used a transmitter frequency of 8 kHz. A total of 7 sub-bottom sonar profiles were acquired (Figure 2). At shallow depths, the seafloor was also observed visually to distinguish between sedimentary, rocky, and seagrass-covered seabed. The sub-bottom profiles were visualized and interpreted in the IHS Markit Kingdom software (Version

2018, IHS Markit, London, UK). Two-way travel times (TWT^s; in milliseconds) of the seafloor (sf^{TWT}) and the top of the weathered/compact bedrock (d^{TWT}) were determined at borehole locations (Table 2).

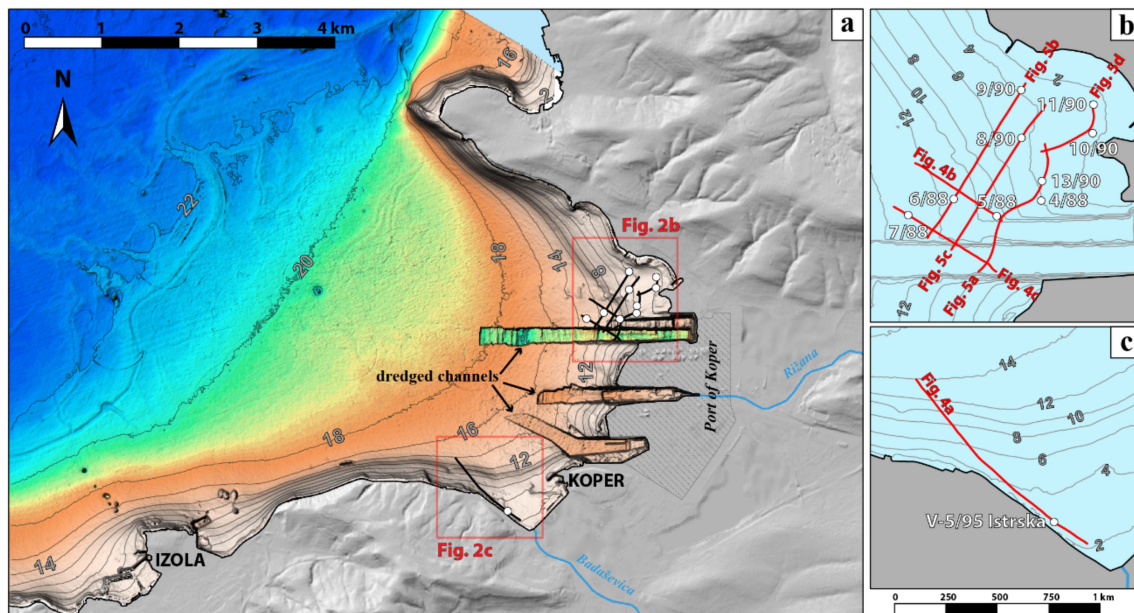


Figure 2. Study area. (a) Bay of Koper with borehole (white circles) and sub-bottom sonar profile locations (thick black lines). (b) and (c) close-ups of the studied areas with bathymetry indicated by thin grey lines. Red lines show the locations of sub-bottom sonar profiles presented in Figures 3 and 4. White circles indicate borehole locations. For clarity the “A-III-” prefix is not shown in (b).

Table 1. Boreholes used in this study (GeoZS: Geological Survey of Slovenia; IGGG: Institute for Geology, Geotechnics and Geophysics Ljubljana).

Borehole Name	Geographical Coordinates		Seafloor Depth [m b.s.l.]	Borehole Length [m]	Drill Period	Orthogonal Distance to the Nearest Sonar Profile [m]	Contractor
	Latitude	Longitude					
A-III-4/88	45°34'4.2119"	13°44'11.0875"	4.8	22.0	December 1988	22.0	GeoZS
A-III-5/88	45°34'1.6538"	13°44'1.1537"	7.0	24.0	November 1988	0.5	GeoZS
A-III-6/88	45°34'4.2390"	13°43'51.4528"	8.0	23.0	December 1988	1.5	GeoZS
A-III-7/88	45°34'1.5963"	13°43'41.2889"	15.0	20.0	December 1988	1.0	GeoZS
A-III-8/90	45°34'14.0408"	13°44'6.4254"	5.1	21.0	November 1990	1.0	GeoZS
A-III-9/90	45°34'21.5862"	13°44'6.2099"	4.4	18.0	November 1990	1.5	GeoZS
A-III-10/90	45°34'14.9625"	13°44'22.4093"	2.4	20.0	November 1990	23.5	GeoZS
A-III-11/90	45°34'19.4662"	13°44'22.4931"	2.1	16.0	November 1990	8.5	GeoZS
A-III-13/90	45°34'7.2908"	13°44'11.1891"	4.9	27.0	November 1990	3.5	GeoZS
V-5/95 Istrska	45°32'40.5603"	13°42'56.0674"	4.5	10.0	November 1995	2.5	IGGG

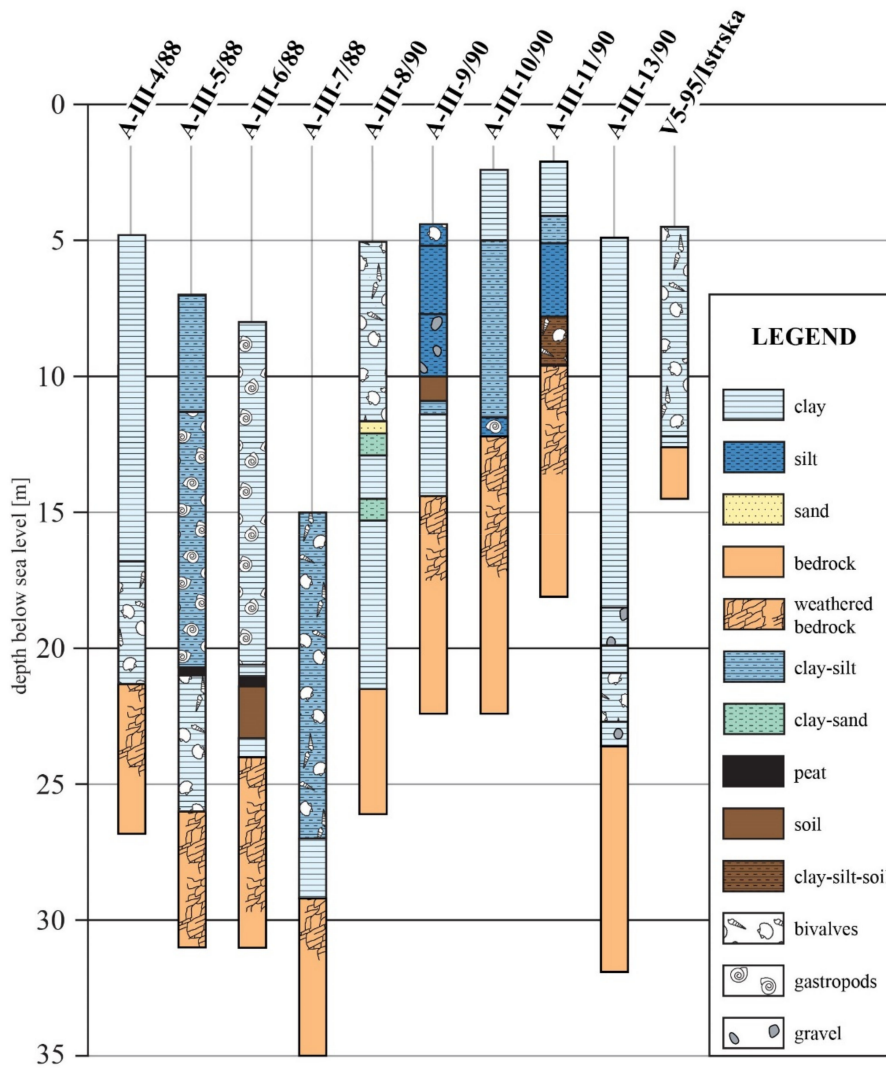


Figure 3. Sub-bottom sonar profiles (with superimposed boreholes) where the top of the Eocene bedrock is expressed as a single undulating medium-to-high amplitude reflection ((a), (b) and (c)). For profile locations, see Figure 2. Blue overlay marks the Quaternary sediment and orange overlay marks the bedrock. Peat layers are indicated with brown arrows. Red overlay within the Quaternary section marks isolated diffraction hyperbolas. Red overlay in the water column marks reflection events above the seafloor. Green overlay marks the extent of seagrass meadows on the seafloor. Dredged areas are marked with grey arrows. Multiples are indicated by thin black arrows.

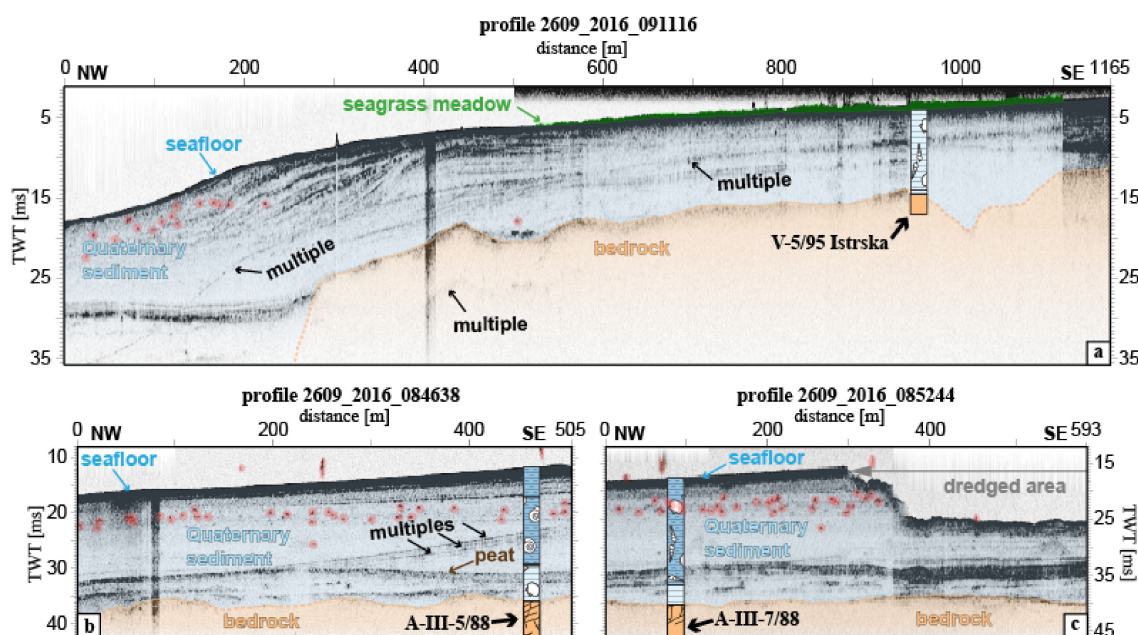


Figure 4. Sub-bottom sonar profiles (with superimposed boreholes) where the top of the Eocene succession is expressed as a medium-to-high amplitude reflection unit with a well-definable top from which downward shallow-dipping reflections emerge ((a–c)). For profile locations, see Figure 2. For an explanation of the color overlays, the reader is referred to Figure 3.

Table 2. Thickness of Quaternary sediments at borehole locations from borehole logs (th^b) and sonar profiles (th^{TWT}), the depth of the seafloor (sf^{TWT}), and the top of the bedrock (d^{TWT}) from the sonar profiles and the calculated average sound velocity in Quaternary sediments at the borehole location.

Borehole Name	From Borehole Logs	From Sonar Profiles			Average Sound Velocity in Quaternary Sediments at the Borehole Location [m/s]	Orthogonal Distance to the Nearest Sonar Profile [m]
	th^b [m]	sf^{TWT} [ms]	d^{TWT} [ms]	th^{TWT} [ms]		
A-III-4/88	16.5	6.4	29.9	23.5	1404.3	22.0
A-III-5/88	19.0	11.5	36.0	24.5	1551.0	0.5
A-III-6/88	16.0	15.0	36.0	21.0	1523.8	1.5
A-III-7/88	14.2	17.5	40.2	22.7	1251.1	1.0
A-III-8/90	16.4	6.4	25.4	19.0	1726.3	1.0
A-III-9/90	10.0	5.1	17.7	12.6	1587.3	1.5
A-III-10/90	9.8	2.8	17.0	14.2	1380.3	23.5
A-III-11/90	7.5	3.0	11.9	8.9	1685.4	8.5
A-III-13/90	18.7	5.0	28.4	23.4	1598.3	3.5
V-5/95 Istrska	8.1	4.0	14.6	10.6	1528.3	2.5

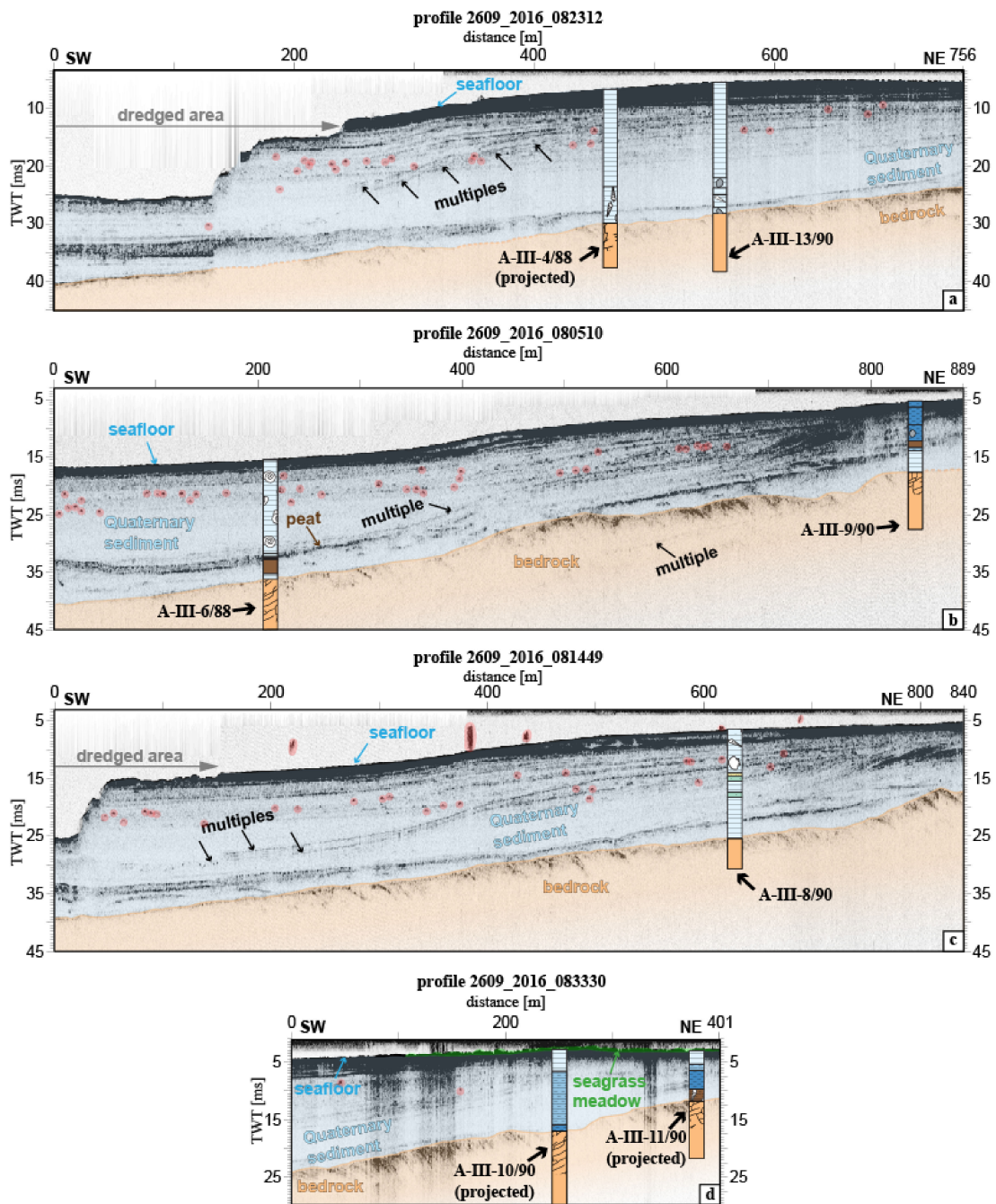


Figure 5. Borehole logs determined from geotechnical reports (see Section 2).

The thickness of Quaternary sediments in the borehole (th^b , in meters) was derived from the geotechnical reports and was calculated as the depth from the top of the core to the top of the bedrock represented by weathered or compact Eocene turbidites (see Figure 5). The thickness of Quaternary sediments from the sub-bottom profiles (th^{TWT} , in milliseconds) was obtained by subtracting the TWTs from the top of the bedrock (d^{TWT} , in milliseconds) and the sea floor (sf^{TWT} , in milliseconds) at the borehole location (see Figures 3 and 4; Table 2). When the profiles did not directly overlie the borehole (Figure 2b and Table 1), the part of the profile closest to the borehole was used to determine th^{TWT}

(Figure 4a,d). The average sound velocity in Quaternary sediments at the borehole location (v , in meters per second; Table 2) was calculated using the following formula:

$$v = \frac{2 \times 10^3 \times th^b}{th^{TWT}}. \quad (1)$$

3. Results

3.1. Boreholes

Borehole logs are provided in Figure 5. The Quaternary succession (including the Holocene marine sediment) is composed of fine-grained clastics with occasional gravelly horizons. Only core A-III-8/90 contains sandy horizons. Soil-rich and peat horizons are present in some of the boreholes. Horizons with bivalves and/or gastropods occur in all boreholes; however, no remarks on the species or their environment are provided in the borehole geotechnical reports. Due to the lack of detailed descriptions of the boreholes, we did not attempt to interpret the sedimentary environments. However, it is clear that the Quaternary sediments comprise terrestrial-marine deposits. The bottom parts of all the boreholes consist of weathered and/or compact bedrock built of Eocene interbedded sandstones and marlstones.

3.2. Sub-Bottom Sonar Profiles

The sub-bottom profiles with superimposed boreholes are shown in Figures 3 and 4. Boreholes more than 5 m away from the nearest sub-bottom profile were projected orthogonally to the profile (Table 1, Figure 4a,d). The seafloor is marked by the first strong sub-horizontal reflection and is indicated by a blue arrow. The Quaternary sequence is indicated by a light blue overlay. Quaternary sediments are seen as (1) acoustically transparent units (Figures 3 and 4), (2) units containing onlapping or concordant reflection geometries (Figures 3 and 4), and (3) units with sigmoidal (prograding) reflection configurations (Figures 3a and 4b,c). Eocene bedrock is indicated by a light orange overlay. The often undulating unconformity at the top of the bedrock is expressed as (1) a medium-to-high amplitude reflection under which deeper reflections are not observed (Figure 3) or (2) an up to 5 ms TWT thick medium-to-high amplitude reflection unit with a well-definable top from which downward short shallow-dipping reflections emerge (Figure 4). The acoustic record does not discriminate between weathered or compact bedrock.

In addition to the two described units, the sub-bottom profiles contain several other features. Columnar-shaped reflections (gas flares) within the seawater column are located above the seafloor and are indicated by a light red overlay in Figure 3b,c and Figure 4c. Rough seafloor morphologies with plentiful diffraction hyperbolas are observed above the dredged areas (Figure 2a,b, Figures 3c and 4a,c), which were excavated to accommodate ships with larger drafts in the Port of Koper. Slightly rougher seafloor morphologies are also produced by seagrass (most commonly *Posidonia* sp.) meadows (marked by a light green overlay in Figures 3a and 4d), which were visually recognized during sub-bottom sonar acquisition. Significant, yet variable reflection degradation is seen directly beneath the areas covered by seagrass. Within the Quaternary sedimentary column, peat layers produce medium-to-high amplitude, sub-horizontal, 1–2 ms TWT thick reflections (Figures 3b and 4b). All sonar profiles show many small diffraction hyperbolas scattered between 25 and 15 ms TWTs within the sedimentary column (Figures 3 and 4). Seafloor multiples appear on the majority of the profiles (Figure 3a,b and Figure 4a–c) due to the shallow acquisition depths. Figure 3a also contains a multiple of the top of the bedrock.

3.3. Average Sound Velocity in Quaternary Sediments

Thicknesses of Quaternary sediments from drilling reports and geophysical data along with the calculated average sound velocities at borehole locations are provided in Table 2. The mean, median, and standard deviation for the whole dataset are 1523.6 m/s, 1539.7 m/s, and 144.0, respectively.

4. Discussion

4.1. Sound Velocity Variation

The sound velocity variation in the presented dataset is significant (Section 3.3). Some of the calculated velocity values can be considered less reliable due to significant distance between the respective borehole and its closest sub-bottom sonar profile (Table 2). If we omit the two boreholes that are separated by more than 20 m from their nearest sub-bottom profile (A-III-4/88 and A-III-10/90), the mean, median, and standard deviation for the dataset become 1556.4 m/s, 1569.2 m/s, and 143.1, respectively. Since the standard deviation remains relatively high, we discuss the principal influences on the sound velocity scattering below.

4.1.1. Influence of Overburden

Sound velocity in sediments strongly depends on porosity, which is in turn influenced by overburden and compaction [1,4]. Here, the overburden comprises the combined weight of the water and sedimentary columns at the borehole locations. In Figure 6, we plot the calculated velocity against the thickness of Quaternary sediments taken from borehole logs and sonar profiles (a proxy for the weight of the sedimentary column), the depth of the seafloor taken from sonar profiles (a proxy for the weight of the water column), and the depth of the top of the bedrock taken from sonar profiles (a proxy for the weight of the water and sedimentary column). A strong scattering of plotted data points demonstrates that there is no relation between the determined sound velocity and these parameters. Additionally, in the correlation plots, the x -axis values of the minimum (red) and maximum sound velocities (green) are often quite similar (Figure 6a,c,d), again suggesting that velocities are uncorrelated to the overburden thickness. This shows that, in thin sedimentary successions located in shallow water depths, overburden does not significantly influence the sound velocity.

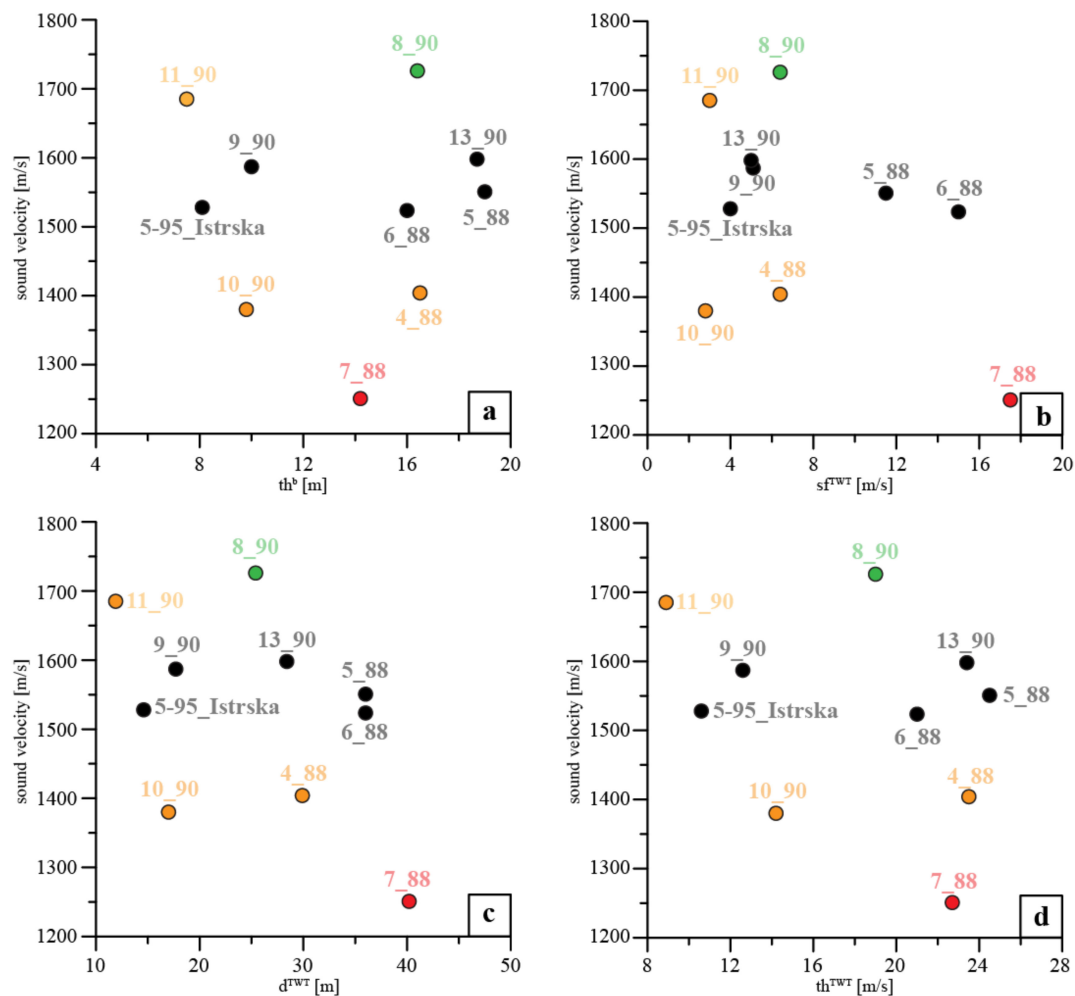


Figure 6. Plots of sound velocity versus (a) the thickness of Quaternary sediments (taken from borehole logs), (b) the depth of the seafloor (taken from sonar profiles), (c) the depth of the top of the bedrock (taken from sonar profiles), and (d) the thickness of Quaternary sediments (taken from sonar profiles). For clarity, A-III- and V- prefixes are removed from borehole labels. Data points in orange mark less reliable velocities (boreholes more than 5 m away from the nearest sub-bottom sonar profile; Table 2 and Figure 2b). Data points in green and red mark the maximum and minimum calculated velocities (Table 2).

4.1.2. Influence of Grain Size

The influence of mean grain size on sound velocity in surficial marine sediments is well known [4,5,19,83,84]. Although granulometric analyses of the cored sediments used in our study were unavailable, general grain size classes could still be determined from borehole geotechnical logs (see Section 2). Therefore, an estimation of the influence of grain size on the sound velocity in our dataset is possible. In Figure 7, the calculated sound velocities at our study site were added to the plot, correlating sound velocity with the mean grain size of surficial sediments of continental shelves from [19]. Clearly, our calculated velocities (at boreholes located close to the acquired profiles) correspond well with the expected sound velocity range of the predominant grain size class determined from the borehole logs (Figures 5 and 7), even though the dataset of [19] is based on surficial sediment samples. Boreholes penetrating exclusively clay (A-III-6/88 and V5/95 Istrska) are in the lower sound velocity spectra, whereas boreholes mainly encountering silt (A-III-5/88, A-III-9/90 and A-III-11/90) are in the middle velocity spectra, corresponding to silt mean grain size velocities. Maximum sound velocity was calculated for Borehole A-III-8/90, which is the only core containing sandy sediment. Although clay

dominates in this borehole, the amount of sandy sediment seems to be sufficient enough to significantly increase the average velocity in the Quaternary succession. A special case is presented by Borehole A-III-13/90, which penetrated clay; however, its calculated velocity corresponds to the mean grain sizes of silt. This discrepancy can be attributed to (1) an inadequate geotechnical description of the core, (2) an abrupt increase in sound velocity within the gravelly horizons (Figure 5), or (3) the presence of an overconsolidated layer within the sequence. In conclusion, the generally good agreement between the calculated velocities and expected velocities for the predominant grain size classes indicates that the composition of the stratal succession is a major factor influencing velocity variations in our study area.

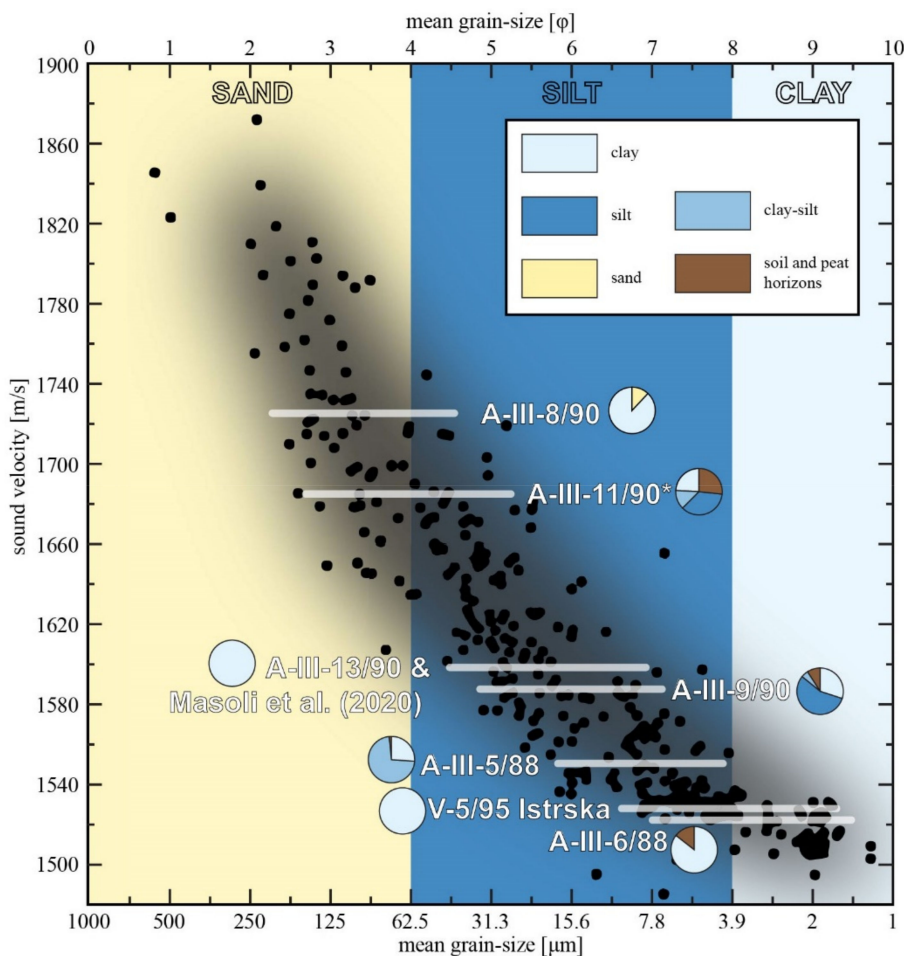


Figure 7. The relation between sound velocity and mean grain size for continental shelf sediments (after [19]) with added velocities from our study. Our estimated sound velocities and the velocity value from [76] for a similar setting in the Gulf of Trieste (see Section 4.3) are shown by white horizontal overlays. Asterisk at Borehole A-III-11/90 indicates that this borehole is separated by more than 5 m from the nearest sub-bottom profile. Pie charts display the proportions of sediment types in each borehole core (for details, see Figure 5).

4.1.3. Influence of Gas Presence

Abundant diffraction hyperbolas are present within the Quaternary succession (Figures 3 and 4; Section 3.2). They could be produced by reflections from gravel horizons; however, their occurrence does not correlate with gravel layers determined in the boreholes (Figures 3 and 4). The diffraction hyperbolas more likely indicate low concentrations of gas in the sedimentary column, commonly encountered in high-resolution geophysical profiles [85–87]. Reflective features in the water column (Figure 3b,c and Figure 4c; Section 3.2), which commonly result from gas-bubble plumes emitting from the seafloor [88–90], further indicate gas occurrence. The lowest sound velocity in our dataset was

calculated for Borehole A-III-7/88, which penetrates a hyperbola-dense zone clearly visible on the corresponding sub-bottom sonar profile (Table 2 and Figure 3c). Since even minor gas concentrations (1–2%) dramatically reduce sound velocity in sediments [83,84,91–93], we attribute this significantly lower velocity value to gas in the Quaternary sediment. In the northern Adriatic seabed, gas seeps are commonly observed and are attributed to both deep and shallow sources [94–98]. Since the diffraction hyperbolas in our sonar profiles are constrained only to a narrow zone in the uppermost part of the Quaternary sequence (Figures 3 and 4), we propose that the gas (probably methane) originates from a degradation of organic matter contained in the Holocene paralic and marine sediments and/or Late Pleistocene terrestrial sequences [62,97,99]. Gas production related to biological processes in seagrass meadows can also greatly hinder the propagation of acoustic signals [100–102]; however, the contribution of this effect is difficult to determine from our dataset since only a single borehole (V-5/95) is located within a meadow (Figure 3a). Nevertheless, significant signal attenuation below the meadows can be observed in the geophysical data (Section 3.2, Figures 3a and 4d).

4.2. Are Average Sound Velocities an Oversimplification?

Using average sound velocities for depth conversion of a highly heterogeneous Quaternary succession can be considered a gross oversimplification as the velocity strongly varies with grain size [4,5,19,83,84]. However, when comparing the sub-bottom sonar profiles and the borehole logs used in our study (Figure 5, Figure 3, and Figure 4), a good alignment between the reflections and the main sedimentological boundaries from the borehole logs is apparent (Figure 3b,c and Figure 4a,b). Especially peat layers prove to be very effective reflectors, which has already been noted in the northern Adriatic Sea by other authors [43,47,50–52,76,97,103,104]. This demonstrates that average velocity can be quite effectively used for robust depth conversion of sonar profiles in thin and shallow Quaternary successions.

4.3. Comparison with the Sound Velocity from the Bay of Muggia

An earlier study in a similar geological setting [76] reported sound velocity in Late Quaternary sediments from the neighboring Bay of Muggia (Figure 1b), which comprise Rosandra river deposits submerged in the Holocene transgression. There, the Quaternary succession is between 20 and 30 m thick and is composed of clay and silt with occasional sand and peat horizons. The water depth extends between 18 and 21 m. The Bay of Muggia site is therefore quite similar to our study site both in sediment thickness and composition. Using P-wave seismic refraction [76] led to a sound velocity value of 1595 m/s, which fits within the range of velocities estimated in our study (Figure 7). This implies that, also in the Bay of Muggia, the sound velocity in the Quaternary sediment is largely controlled by the sediment type and further corroborates sedimentary type as the major factor influencing sound velocity in shallow, thin, terrestrial-marine Quaternary sedimentary environment successions.

4.4. Choosing the Appropriate Velocity for the Depth Conversion of Geophysical Data

The results of our study show that sound velocity in thin (up to 20 m thick) submerged terrestrial-marine Quaternary successions located in near-shore areas few tens of meters deep is mostly controlled by the predominant grain size class of the succession (Section 4.1.2). The sound velocity for depth conversion in these settings can be chosen based on the predominant grain size class. We show that the sound velocity vs. grain size relationships previously documented in surficial sediments [19] are also valid for buried and submerged Quaternary successions (Section 4.1.2). Therefore, published values for sound velocity of surficial sediments can be utilized for depth conversion of shallow offshore high-resolution geophysical data, as long as the selected grain size corresponds to the predominant grain size class of the Quaternary succession.

Terrestrial-marine Quaternary successions often contain significant amounts of degrading organic matter; consequently, locally present gas further influences sound velocity in these settings (Section 4.1.3). Different gas indicators can easily be recognized from high-resolution geophysical data [85–93],

facilitating the mapping of low-velocity areas. As the velocity decrease associated with the presence of gas is often quite variable e.g., [93], we suggest avoiding detailed velocity analysis in gas-rich areas.

5. Conclusions

We used geophysical and borehole data to determine sound velocities through the Quaternary fill of a submerged alluvial plain containing terrestrial, paralic, and marine sediments. Our study shows that an average sound velocity through the Quaternary sedimentary column is sufficient for depth conversion of high-resolution geophysical profiles acquired in thin (up to 20 m thick) Quaternary successions in shallow (up to 20 m) water depths. We find that, in these settings, the main factor influencing sound velocity is the sediment type (i.e. mean grain size) contained within the studied sedimentary column, whereas overburden effects do not show any influence. However, where gas is present in the sedimentary column, it reduces sound velocity by a few hundred meters per second and becomes the dominant factor influencing sound velocity.

We found that, for a good approximation of the average sound velocity at a borehole, the velocity typical for the most represented sediment type in the borehole column can be employed. Nevertheless, in highly heterogeneous sedimentary settings, such as the Bay of Koper investigated in this study, significant lateral variations in average velocity will occur within a small area, necessitating a careful selection of multiple, most representative values, if relying on velocities published in the literature.

Using our study area in the northern Adriatic, we provided reference values for sound velocity in thin, mud-dominated Quaternary sedimentary successions in shallow coastal areas. Velocity values determined in our study correlate well with the sound velocity vs. grain size relationships previously documented in surficial sediments [19], showing that these published values can also be used for shallow sub-bottom sedimentary sequences.

Author Contributions: All authors have read and agree to the published version of the manuscript. Conceptualization: A.N. and M.V.; methodology: A.N.; validation: A.N.; formal analysis: A.N.; investigation: A.N., S.P., and B.C.; resources: S.P. and B.C.; writing—original draft preparation: A.N.; writing—review and editing: A.N., A.Š., S.P., B.C., and M.V.; visualization: A.N.; supervision: M.V.; project administration: A.N. and M.V.; funding acquisition: M.V.

Funding: This research was funded by: the Slovenian Research Agency, Young Researcher grant number 38136; the Slovenian Research Agency and Harpha Sea d.o.o., grant number L1-5452; the Slovenian Research Agency, grant number J1-1712; the Slovenian Research Agency, research programme P1-0195. The APC was funded by the Slovenian Research Agency, research programme P1-0195.

Acknowledgments: This work was supported by the Slovenian Research Agency (Young Researcher grant Nr. 38136), by joint funding of the Slovenian Research Agency and Harpha Sea d.o.o. within the project L1-5452 (Application of sonar in research of active tectonics and paleoseismology in low-strain environments) and by funding of the Slovenian Research Agency within the project J1-1712 (Record of environmental change and human impact in Holocene sediments, Gulf of Trieste) and within the research programme P1-0195 (Geoenvironment and Geomaterials). We would like to acknowledge IHS Markit Kingdom and their University Education Grant, which provided us with IHS Markit Kingdom software licences. The crew of the vessel Lyra (Iztok Rant and Rok Soczka Mandac) is acknowledged for their assistance and hospitality during sub-bottom acquisition. We would also like to thank Karoly Nemeth and an anonymous reviewer for their comments, which allowed us to improve the manuscript.

Conflicts of Interest: The authors declare that there is no conflict of interest. The funders had no role in the design of the study; in the collection, analyses, or interpretation of data; in the writing of the manuscript; or in the decision to publish the results.

References

1. Sheriff, R.E.; Geldart, L.P. *Exploration Seismology*, 2nd ed.; Cambridge University Press: Cambridge, UK, 1995.
2. Endler, M.; Endler, R.; Bobertz, B.; Leipe, T.; Arz, H.W. Linkage between acoustic parameters and seabed sediment properties in the south-western Baltic Sea. *GeoMar. Lett.* **2015**, *35*, 145–160. [[CrossRef](#)]
3. Endler, M.; Endler, R.; Wunderlich, J.; Bobertz, B.; Leipe, T.; Moros, M.; Jensen, J.B.; Arz, H.W. Geo-acoustic modelling of late and postglacial sedimentary units in the Baltic Sea and their acoustic visibility. *Mar. Geol.* **2016**, *376*, 86–101. [[CrossRef](#)]

4. Jackson, D.R.; Richardson, M.D. *High-Frequency Seafloor Acoustics*; Springer: Berlin/Heidelberg, Germany, 2007; ISBN 0387369457.
5. Hamilton, E.L. Geoacoustic modeling of the sea floor. *J. Acoust. Soc. Am.* **1980**, *68*, 1313–1340. [[CrossRef](#)]
6. Brandes, H.G.; Silva, A.J.; Sadd, M.H. Physical and acoustic measurements on cohesionless sediments from the northwest Florida Sand Sheet. *Geophys. Res. Lett.* **2001**, *28*, 823–826. [[CrossRef](#)]
7. Kan, G.; Liu, B.; Wang, J.; Meng, X.; Li, G.; Hua, Q.; Sun, L. Sound speed dispersion characteristics of three types of shallow sediments in the southern yellow sea. *Mar. Georesources Geotechnol.* **2018**, *36*, 853–860. [[CrossRef](#)]
8. Kim, D.C.; Sung, J.Y.; Park, S.C.; Lee, G.H.; Choi, J.H.; Kim, G.Y.; Seo, Y.K.; Kim, J.C. Physical and acoustic properties of shelf sediments, the South Sea of Korea. *Mar. Geol.* **2001**, *179*, 39–50. [[CrossRef](#)]
9. Kim, G.Y.; Park, K.J.; Lee, G.S.; Yoo, D.G.; Kong, G.S. Physical property characterization of quaternary sediments in the vicinity of the paleo-Seomjin River of the continental shelf of the South Sea, Korea. *Quat. Int.* **2018**, *503*, 153–162. [[CrossRef](#)]
10. Kim, S.R.; Lee, G.-S.; Kim, D.C.; Bae, S.H.; Kim, S.-P. Physical properties and geoacoustic provinces of surficial sediments in the southwestern part of the Ulleung Basin in the East Sea. *Quat. Int.* **2017**, *459*, 35–44. [[CrossRef](#)]
11. Richardson, M.D.; Lavoie, D.L.; Briggs, K.B. Geoacoustic and physical properties of carbonate sediments of the Lower Florida Keys. *Geo Mar. Lett.* **1997**, *17*, 316–324. [[CrossRef](#)]
12. Zhang, Y.; Guo, C.; Wang, J.; Hou, Z.; Chen, W. Relationship between in situ sound velocity and granular characteristics of seafloor sediments in the Qingdao offshore region. *Chin. J. Oceanol. Limnol.* **2017**, *35*, 704–711. [[CrossRef](#)]
13. Zheng, J.; Liu, B.; Kan, G.; Li, G.; Pei, Y.; Liu, X. The sound velocity and bulk properties of sediments in the Bohai Sea and the Yellow Sea of China. *Acta Oceanol. Sin.* **2016**, *35*, 76–86. [[CrossRef](#)]
14. Wang, J.; Guo, C.; Liu, B.; Hou, Z.; Han, G. Distribution of geoacoustic properties and related influencing factors of surface sediments in the southern South China Sea. *Mar. Geophys. Res.* **2016**, *37*, 337–348. [[CrossRef](#)]
15. Richardson, M.D.; Briggs, K.B. In situ and laboratory geoacoustic measurements in soft mud and hard-packed sand sediments: Implications for high-frequency acoustic propagation and scattering. *Geo Mar. Lett.* **1996**, *16*, 196–203. [[CrossRef](#)]
16. Gorgas, T.J.; Wilkens, R.H.; Fu, S.S.; Frazer, L.N.; Richardson, M.D.; Briggs, K.B.; Lee, H. In situ acoustic and laboratory ultrasonic sound speed and attenuation measured in heterogeneous soft seabed sediments: Eel River shelf, California. *Mar. Geol.* **2002**, *182*, 103–119. [[CrossRef](#)]
17. Kim, G.Y.; Narantsetseg, B.; Lee, J.Y.; Chang, T.S.; Lee, G.S.; Yoo, D.G.; Kim, S.P. Physical and geotechnical properties of drill core sediments in the Heuksan Mud Belt off SW Korea. *Quat. Int.* **2018**, *468*, 33–48. [[CrossRef](#)]
18. Orsi, T.H.; Dunn, D.A. Correlations between sound velocity and related properties of glacio-marine sediments: Barents sea. *GeoMar. Lett.* **1991**, *11*, 79–83. [[CrossRef](#)]
19. Hamilton, E.L.; Bachman, R.T. Sound velocity and related properties of marine sediments. *J. Acoust. Soc. Am.* **1982**, *72*, 1891–1904. [[CrossRef](#)]
20. Bae, S.H.; Kim, D.C.; Lee, G.S.; Kim, G.Y.; Kim, S.P.; Seo, Y.K.; Kim, J.C. Physical and acoustic properties of inner shelf sediments in the South Sea, Korea. *Quat. Int.* **2014**, *344*, 125–142. [[CrossRef](#)]
21. Waelbroeck, C.; Labeyrie, L.; Michel, E.; Duplessy, J.C.; Lambeck, K.; McManus, J.F.; Balbon, E.; Labracherie, M. Sea-level and deep water temperature changes derived from benthic foraminifera isotopic records. *Quat. Sci. Rev.* **2002**, *21*, 295–305. [[CrossRef](#)]
22. Lambeck, K.; Rouby, H.; Purcell, A.; Sun, Y.; Sambridge, M. Sea level and global ice volumes from the Last Glacial Maximum to the Holocene. *Proc. Natl. Acad. Sci. USA* **2014**, *111*, 15296–15303. [[CrossRef](#)]
23. Allen, G.P.; Posamentier, H.W. Sequence Stratigraphy and Facies Model of an Incised Valley Fill: The Gironde Estuary, France. *Sepm J. Sediment. Res.* **1993**, *63*, 378–391. [[CrossRef](#)]
24. Allen, G.P. Sedimentary processes and facies in the Gironde estuary: A recent model for macrotidal estuarine systems. *Clastic Tidal Sedimentol.* **1991**, *16*, 29–39. [[CrossRef](#)]
25. Cattaneo, A.; Steel, R.J. Transgressive deposits: A review of their variability. *Earth Sci. Rev.* **2003**, *62*, 187–228. [[CrossRef](#)]
26. Sturt, F.; Flemming, N.C.; Carabias, D.; Jöns, H.; Adams, J. The next frontiers in research on submerged prehistoric sites and landscapes on the continental shelf. *Proc. Geol. Assoc.* **2018**, *129*, 654–683. [[CrossRef](#)]

27. Harff, J.; Bailey, G.N.; Lüth, F. Geology and archaeology: Submerged landscapes of the continental shelf: An introduction. *Geol. Soc. Lond. Spec. Publ.* **2016**, *411*, 1–8. [[CrossRef](#)]
28. Brunović, D.; Miko, S.; Hasan, O.; Papatheodorou, G.; Ilijanić, N.; Miseroćchi, S.; Correggiari, A.; Geraga, M. Late Pleistocene and Holocene paleoenvironmental reconstruction of a drowned karst isolation basin (Lošinj Channel, NE Adriatic Sea). *Palaeogeogr. Palaeoclimatol. Palaeoecol.* **2020**, *544*, 109587. [[CrossRef](#)]
29. Benjamin, J.; Rovere, A.; Fontana, A.; Furlani, S.; Vacchi, M.; Inglis, R.H.; Galili, E.; Antonioli, F.; Sivan, D.; Miko, S.; et al. Late Quaternary sea-level changes and early human societies in the central and eastern Mediterranean Basin: An interdisciplinary review. *Quat. Int.* **2017**, *449*, 29–57. [[CrossRef](#)]
30. Bailey, G.N.; Harff, J.; Sakellariou, D. *Under the Sea: Archaeology and Palaeolandscapes of the Continental Shelf*; Springer: Berlin/Heidelberg, Germany, 2017. [[CrossRef](#)]
31. Prins, L.T.; Andresen, K.J. Buried late Quaternary channel systems in the Danish North Sea – Genesis and geological evolution. *Quat. Sci. Rev.* **2019**, *223*, 105943. [[CrossRef](#)]
32. Wiberg-Larsen, P.; Bennike, O.; Jensen, J.B. Submarine Lateglacial lake deposits from the Kattegat, southern Scandinavia. *J. Quat. Sci.* **2019**, *34*, 165–171. [[CrossRef](#)]
33. De Clercq, M.; Missiaen, T.; Wallinga, J.; Zurita Hurtado, O.; Versendaal, A.; Mathys, M.; De Batist, M. A well-preserved Eemian incised-valley fill in the southern North Sea Basin, Belgian Continental Shelf-Coastal Plain: Implications for northwest European landscape evolution. *Earth Surf. Process. Landf.* **2018**, *43*, 1913–1942. [[CrossRef](#)]
34. Cooper, J.A.G.; Green, A.N.; Compton, J.S. Sea-level change in southern Africa since the Last Glacial Maximum. *Quat. Sci. Rev.* **2018**, *201*, 303–318. [[CrossRef](#)]
35. García-Moreno, D.; Gupta, S.; Collier, J.S.; Oggioni, F.; Vanneste, K.; Trentesaux, A.; Verbeeck, K.; Versteeg, W.; Jomard, H.; Camelbeeck, T.; et al. Middle–Late Pleistocene landscape evolution of the Dover Strait inferred from buried and submerged erosional landforms. *Quat. Sci. Rev.* **2019**, *203*, 209–232. [[CrossRef](#)]
36. Kirkpatrick, L.H.; Green, A.N.; Pether, J. The seismic stratigraphy of the inner shelf of southern Namibia: The development of an unusual nearshore shelf stratigraphy. *Mar. Geol.* **2019**, *408*, 18–35. [[CrossRef](#)]
37. Mattei, G.; Troisi, S.; Aucelli, P.; Pappone, G.; Peluso, F.; Stefanile, M. Sensing the Submerged Landscape of Nisida Roman Harbour in the Gulf of Naples from Integrated Measurements on a USV. *Water* **2018**, *10*, 1686. [[CrossRef](#)]
38. Perkins, E.J.; Gorman, A.R.; Tidey, E.J.; Wilson, G.S.; Ohneiser, C.; Moy, C.M.; Riesselman, C.R.; Gilmer, G.; Ross, B.S. High-resolution seismic imaging reveals infill history of a submerged Quaternary fjord system in the subantarctic Auckland Islands, New Zealand. *Quat. Res.* **2019**, *93*, 255–266. [[CrossRef](#)]
39. Laws, A.W.; Maloney, J.M.; Klotsko, S.; Gusick, A.E.; Braje, T.J.; Ball, D. Submerged paleoshoreline mapping using high-resolution Chirp sub-bottom data, Northern Channel Islands platform, California, USA. *Quat. Res.* **2019**, *93*, 1–22. [[CrossRef](#)]
40. García-Moreiras, I.; Cartelle, V.; García-Gil, S.; Muñoz Sobrino, C. First high-resolution multi-proxy palaeoenvironmental record of the Late Glacial to Early Holocene transition in the Ría de Arousa (Atlantic margin of NW Iberia). *Quat. Sci. Rev.* **2019**, *215*, 308–321. [[CrossRef](#)]
41. Pretorius, L.; Green, A.N.; Cooper, J.A.G.; Hahn, A.; Zabel, M. Outer- to inner-shelf response to stepped sea-level rise: Insights from incised valleys and submerged shorelines. *Mar. Geol.* **2019**, *416*, 105979. [[CrossRef](#)]
42. Lambeck, K.; Antonioli, F.; Purcell, A.; Silenzi, S. Sea-level change along the Italian coast for the past 10,000yr. *Quat. Sci. Rev.* **2004**, *23*, 1567–1598. [[CrossRef](#)]
43. Correggiari, A.; Roveri, M.; Trincardi, F. Late Pleistocene and Holocene evolution of the North Adriatic Sea. *Quaternario* **1996**, *9*, 697–704.
44. Ogorelec, B.; Mišič, M.; Šerclj, A.; Cimerman, F.; Faganeli, J.; Stegnar, P. Sediment sečoveljske soline. *Geologija* **1981**, *24*, 180–216.
45. Vacchi, M.; Marriner, N.; Morhange, C.; Spada, G.; Fontana, A.; Rovere, A. Multiproxy assessment of Holocene relative sea-level changes in the western Mediterranean: Sea-level variability and improvements in the definition of the isostatic signal. *Earth Sci. Rev.* **2016**, *155*, 172–197. [[CrossRef](#)]
46. Ronchi, L.; Fontana, A.; Correggiari, A. Characteristics and potential application of Holocene Tidal Inlets in the Northern Adriatic Shelf (Italy). *Alp. Mediterr. Quat.* **2018**, *31*, 31–34.
47. Ronchi, L.; Fontana, A.; Correggiari, A.; Asioli, A. Late Quaternary incised and infilled landforms in the shelf of the northern Adriatic Sea (Italy). *Mar. Geol.* **2018**, *405*, 47–67. [[CrossRef](#)]

48. Zecchin, M.; Ceramicola, S.; Lodolo, E.; Casalbore, D.; Chiocci, F.L. Episodic, rapid sea-level rises on the central Mediterranean shelves after the Last Glacial Maximum: A review. *Mar. Geol.* **2015**, *369*, 212–223. [[CrossRef](#)]
49. Zecchin, M.; Gordini, E.; Ramella, R. Recognition of a drowned delta in the northern Adriatic Sea, Italy: Stratigraphic characteristics and its significance in the frame of the early Holocene sea-level rise. *Holocene* **2015**, *25*, 1027–1038. [[CrossRef](#)]
50. Moscon, G.; Correggiari, A.; Stefani, C.; Fontana, A.; Remia, A. Very-high resolution analysis of a transgressive deposit in the Northern Adriatic Sea (Italy). *Alp. Mediterr. Quat.* **2015**, *28*, 121–129.
51. Correggiari, A.; Field, M.E.; Trincardi, F. Late Quaternary transgressive large dunes on the sediment-starved Adriatic shelf. *Geol. Soc. Lond. Spec. Publ.* **1996**, *117*, 155–169. [[CrossRef](#)]
52. Trincardi, F.; Correggiari, A.; Roveri, M. Late Quaternary transgressive erosion and deposition in a modern epicontinental shelf: The Adriatic semienclosed basin. *GeoMar. Lett.* **1994**, *14*, 41–51. [[CrossRef](#)]
53. Storms, J.E.A.; Weltje, G.J.; Terra, G.J.; Cattaneo, A.; Trincardi, F. Coastal dynamics under conditions of rapid sea-level rise: Late Pleistocene to Early Holocene evolution of barrier-lagoon systems on the northern Adriatic shelf (Italy). *Quat. Sci. Rev.* **2008**, *27*, 1107–1123. [[CrossRef](#)]
54. Ronchi, L.; Fontana, A.; Correggiari, A.; Remia, A. Anatomy of a transgressive tidal inlet reconstructed through high-resolution seismic profiling. *Geomorphology* **2019**, *343*, 65–80. [[CrossRef](#)]
55. Novak, A.; Šmuc, A.; Poglajen, S.; Vrabec, M. Linking the high-resolution acoustic and sedimentary facies of a transgressed Late Quaternary alluvial plain (Gulf of Trieste, northern Adriatic). *Mar. Geol.* **2020**, *419*, 106061. [[CrossRef](#)]
56. Trobec, A.; Šmuc, A.; Poglajen, S.; Vrabec, M. Submerged and buried Pleistocene river channels in the Gulf of Trieste (Northern Adriatic Sea): Geomorphic, stratigraphic and tectonic inferences. *Geomorphology* **2017**, *286*, 110–120. [[CrossRef](#)]
57. Covelli, S.; Fontolan, G.; Faganeli, J.; Ogrinc, N. Anthropogenic markers in the Holocene stratigraphic sequence of the Gulf of Trieste (northern Adriatic Sea). *Mar. Geol.* **2006**, *230*, 29–51. [[CrossRef](#)]
58. Trincardi, F.; Argnani, A.; Correggiari, A.; Fogliani, F.; Rovere, M.; Angeletti, L.; Asioli, A.; Campiani, E.; Cattaneo, A.; Gallerani, A.; et al. *Note illustrative della Carta Geologica dei mari italiani alla scala 1:250.000 foglio NL 33-7 Venezia*; Istituto di Scienze Marine Consiglio Nazionale delle Ricerche: Ancona, Italy, 2011.
59. Trobec, A.; Buseti, M.; Zgur, F.; Baradello, L.; Babich, A.; Cova, A.; Gordini, E.; Romeo, R.; Tomini, I.; Poglajen, S.; et al. Thickness of marine Holocene sediment in the Gulf of Trieste (northern Adriatic Sea). *Earth Syst. Sci. Data* **2018**, *10*, 1077–1092. [[CrossRef](#)]
60. Chiocci, F.L.; Casalbore, D.; Marra, F.; Antonioli, F.; Romagnoli, C. *Relative Sea Level Rise, Palaeotopography and Transgression Velocity on the Continental Shelf*; Springer Cham: Berlin/Heidelberg, Germany, 2017; pp. 39–51. [[CrossRef](#)]
61. Mautner, A.K.; Gallmetzer, I.; Haselmair, A.; Schnedl, S.M.; Tomašových, A.; Zuschin, M. Holocene ecosystem shifts and human-induced loss of Arca and Ostrea shell beds in the north-eastern Adriatic Sea. *Mar. Pollut. Bull.* **2018**, *126*, 19–30. [[CrossRef](#)] [[PubMed](#)]
62. Ogrinc, N.; Faganeli, J.; Ogorelec, B.; Čermelj, B. The origin of organic matter in Holocene sediments in the Bay of Koper (Gulf of Trieste, northern Adriatic Sea). *Geologija* **2007**, *50*, 179–187. [[CrossRef](#)]
63. Tomašových, A.; Gallmetzer, I.; Haselmair, A.; Kaufman, D.S.; Mavrič, B.; Zuschin, M. A decline in molluscan carbonate production driven by the loss of vegetated habitats encoded in the Holocene sedimentary record of the Gulf of Trieste. *Sedimentology* **2019**, *66*, 781–807. [[CrossRef](#)] [[PubMed](#)]
64. Gallmetzer, I.; Haselmair, A.; Tomašových, A.; Mautner, A.-K.; Schnedl, S.-M.; Cassin, D.; Zonta, R.; Zuschin, M. Tracing origin and collapse of Holocene benthic baseline communities in the northern Adriatic Sea. *Palaios* **2019**, *34*, 121–145. [[CrossRef](#)]
65. Pleničar, M. *Osnovna geološka karta SFRJ. L 33-88, Trst*; Zvezni Geološki Zavod: Beograd, Yugoslavia, 1969.
66. Pleničar, M.; Polšak, A.; Šikič, D. *Osnovna Geološka Karta SFRJ. 1:100.000. Tolmač Za List Trst: L 33-88*; Zvezni Geološki Zavod: Beograd, Yugoslavia, 1973.
67. Vrabec, M.; Buseti, M.; Zgur, F.; Facchin, L.; Pelos, C.; Romeo, R.; Sormani, L.; Slavec, P.; Tomini, I.; Visnovic, G.; et al. Refleksijske Seizmične Raziskave v Slovenskem Morju Slomartec 2013. In Proceedings of the Raziskave s Področja Geodezije in Geofizike 2013, Ljubljana, Slovenia, 30 January 2014; Kuhar, M., Čop, R., Gosar, A., Kobold, M., Kralj, P., Malačič, V., Rakovec, J., Skok, G., Stopar, B., Vreča, P., Eds.; University of Ljubljana: Ljubljana, Slovenia, 2014; pp. 97–101.

68. Ogorelec, B.; Faganeli, J.; Mišič, M.; Čermelj, B. Reconstruction of paleoenvironment in the Bay of Koper (Gulf of Trieste, Northern Adriatic). *Annales* **1997**, *11*, 187–200.
69. Ogorelec, B.; Mišič, M.; Faganeli, J. Marine geology of the Gulf of Trieste (northern Adriatic): Sedimentological aspects. *Mar. Geol.* **1991**, *99*, 79–92. [[CrossRef](#)]
70. Ogorelec, B.; Mišič, M.; Faganeli, J.; Šerclj, A.; Cimerman, F.; Dolenc, T.; Pezdič, J. Kvarterni sediment vrstine V-3 v Koprskem zalivu. *Slov. Morje Zaled.* **1984**, *7*, 165–186.
71. Ogorelec, B.; Mišič, M.; Faganeli, J.; Stegnar, P.; Vrišer, B.; Vukovič, A. Recentni sediment Koprškega zaliva. *Geologija* **1987**, *30*, 87–121.
72. Faganeli, J.; Ogorelec, B.; Mišič, M.; Dolenc, T.; Pezdič, J. Organic geochemistry of two 40-m sediment cores from the Gulf of Trieste (Northern Adriatic). *Estuar. Coast. Shelf Sci.* **1987**, *25*, 157–167. [[CrossRef](#)]
73. Covelli, S.; Faganeli, J.; Horvat, M.; Brambati, A. Mercury contamination of coastal sediments as the result of long-term cinnabar mining activity (Gulf of Trieste, northern Adriatic Sea). *Appl. Geochem.* **2001**, *16*, 541–558. [[CrossRef](#)]
74. Žerjal, A.; Kolega, N.; Poglajen, S.; Rant, I.; Jeklar, M.; Lovrič, E.; Vranac, D.; Mozetič, D.; Slavec, P.; Berden Zrimec, M.; et al. *Zajem Naravnih Geomorfoloških Značilnosti Morskega dna, Analiza Antropogenih Fizičnih Poškodb Morskega dna in Klasifikacija Tipov Morskega dna z Določitvijo Obsežnejšega Morskega Rastja na Morskem Dnu*; Harpha Sea: Koper, Slovenia, 2014.
75. EMODnet Bathymetry Consortium. EMODnet Digital Bathymetry (DTM 2018). **2018**. [[CrossRef](#)]
76. Masoli, C.A.; Petronio, L.; Gordini, E.; Deponte, M.; Boehm, G.; Cotterle, D.; Romeo, R.; Barbagallo, A.; Belletti, R.; Maffione, S.; et al. Near-shore geophysical and geotechnical investigations in support of the Trieste Marine Terminal extension. *Near Surf. Geophys.* **2020**, *18*, 73–89. [[CrossRef](#)]
77. *Carta Nautica Da Punta Tagliamento a Pula 1:100 000*; Istituto Idrografico della Marina: Genova, Italy, 2004.
78. Ministry of Transport of the Republic of Slovenia. *Male karte Tržaški zaliv Merilo 1:100 000*; Ministry of Transport of the Republic of Slovenia: Ljubljana, Slovenia, 2005.
79. Placer, L.; Vrabec, M.; Celarc, B. The bases for understanding of the NW Dinarides and Istria Peninsula tectonics. *Geologija* **2010**, *53*, 55–86. [[CrossRef](#)]
80. Jurkovšek, B.; Biolchi, S.; Furlani, S.; Kolar-Jurkovšek, T.; Zini, L.; Jež, J.; Tunis, G.; Bavec, M.; Cucchi, F. Geology of the Classical Karst Region (SW Slovenia–NE Italy). *J. Maps* **2016**, *12*, 352–362. [[CrossRef](#)]
81. Furlani, S.; Finocchiaro, F.; Boschian, G.; Lenaz, D.; Biolchi, S.; Boccali, C.; Monegato, G. Quaternary evolution of the fluviokarst Rosandra valley (Trieste, NE Italy). *Alp. Mediterr. Quat.* **2016**, *29*, 169–179.
82. Biolchi, S.; Furlani, S.; Covelli, S.; Busetti, M.; Cucchi, F. Morphoneotectonics and lithology of the eastern sector of the Gulf of Trieste (NE Italy). *J. Maps* **2016**, *12*, 936–946. [[CrossRef](#)]
83. Anderson, A.L.; Hampton, L.D. Acoustics of gas-bearing sediments. II. Measurements and models. *J. Acoust. Soc. Am.* **1980**, *67*, 1890–1903. [[CrossRef](#)]
84. Anderson, A.L.; Hampton, L.D. Acoustics of gas-bearing sediments I. Background. *J. Acoust. Soc. Am.* **1980**, *67*, 1865–1889. [[CrossRef](#)]
85. Kim, D.C.; Lee, G.S.; Lee, G.H.; Park, S.C. Sediment echo types and acoustic characteristics of gas-related acoustic anomalies in Jinhae Bay, southern Korea. *Geosci. J.* **2008**, *12*, 47–61. [[CrossRef](#)]
86. Visnovitz, F.; Bodnár, T.; Tóth, Z.; Spiess, V.; Kudó, I.; Timár, G.; Horváth, F. Seismic expressions of shallow gas in the lacustrine deposits of Lake Balaton, Hungary. *Near Surf. Geophys.* **2015**, *13*, 433–447. [[CrossRef](#)]
87. Missiaen, T.; Murphy, S.; Loncke, L.; Henriot, J.P. Very high-resolution seismic mapping of shallow gas in the Belgian coastal zone. *Cont. Shelf Res.* **2002**, *22*, 2291–2301. [[CrossRef](#)]
88. Anderson, A.L.; Bryant, W.R. Gassy sediment occurrence and properties: Northern Gulf of Mexico. *GeoMar. Lett.* **1990**, *10*, 209–220. [[CrossRef](#)]
89. Fonseca, L.; Mayer, L.; Orange, D.; Driscoll, N. The high-frequency backscattering angular response of gassy sediments: Model/data comparison from the Eel River Margin, California. *J. Acoust. Soc. Am.* **2002**, *111*, 2621–2631. [[CrossRef](#)]
90. Judd, A.G.; Hovland, M. *Seabed Fluid Flow: The Impact on Geology, Biology and the Marine Environment*; Cambridge University Press: Cambridge, UK, 2007; ISBN 0521819504.
91. Fu, S.S.; Wilkens, R.H.; Frazer, L.N. In situ velocity profiles in gassy sediments: Kiel Bay. *GeoMar. Lett.* **1996**, *16*, 249–253. [[CrossRef](#)]

92. Lee, G.-S.; Kim, D.-C.; Lee, G.-H.; Park, S.-C.; Kim, G.-Y.; Yoo, D.-G.; Kim, J.-C.; Cifci, G. Physical and Acoustic Properties of Gas-bearing Sediments in Jinhae Bay, the South Sea of Korea. *Mar. Georesources Geotechnol.* **2009**, *27*, 96–114. [[CrossRef](#)]
93. Tóth, Z.; Spiess, V.; Mogollón, J.M.; Jensen, J.B. Estimating the free gas content in Baltic Sea sediments using compressional wave velocity from marine seismic data. *J. Geophys. Res. Solid Earth* **2014**, *119*, 8577–8593. [[CrossRef](#)]
94. Donda, F.; Forlin, E.; Gordini, E.; Panieri, G.; Buenz, S.; Volpi, V.; Civile, D.; De Santis, L. Deep-sourced gas seepage and methane-derived carbonates in the Northern Adriatic Sea. *Basin Res.* **2015**, *27*, 531–545. [[CrossRef](#)]
95. Conti, A.; Stefanon, A.; Zuppi, G.M. Gas seeps and rock formation in the northern Adriatic Sea. *Cont. Shelf Res.* **2002**, *22*, 2333–2344. [[CrossRef](#)]
96. Gordini, E.; Falace, A.; Kaleb, S.; Donda, F.; Marocco, R.; Tunis, G. Methane-Related Carbonate Cementation of Marine Sediments and Related Macroalgal Coralligenous Assemblages in the Northern Adriatic Sea. In *Seafloor Geomorphology as Benthic Habitat*; Elsevier: Amsterdam, Netherlands, 2012; pp. 185–200. [[CrossRef](#)]
97. Zecchin, M.; Caffau, M.; Tosi, L. Relationship between peat bed formation and climate changes during the last glacial in the Venice area. *Sediment. Geol.* **2011**, *238*, 172–180. [[CrossRef](#)]
98. Gordini, E.; Marocco, R.; Tunis, G.; Ramella, R. I depositi cementati del Golfo di Trieste (Adriatico Settentrionale): Distribuzione areale, caratteri geomorfologici e indagini acustiche ad alta risoluzione. *Quaternario* **2004**, *17*, 555–563.
99. Ogrinc, N.; Fontolan, G.; Faganeli, J.; Covelli, S. Carbon and nitrogen isotope compositions of organic matter in coastal marine sediments (the Gulf of Trieste, N Adriatic Sea): Indicators of sources and preservation. *Mar. Chem.* **2005**, *95*, 163–181. [[CrossRef](#)]
100. McCarthy, E.M.; Sabol, B. Acoustic characterization of submerged aquatic vegetation: Military and environmental monitoring applications. In Proceedings of the OCEANS 2000 MTS/IEEE Conference and Exhibition, Providence, RI, USA, 11–14 September 2000; 3, pp. 1957–1961. [[CrossRef](#)]
101. Komatsu, T.; Igarashi, C.; Tatsukawa, K.; Sultana, S.; Matsuoka, Y.; Harada, S. Use of multi-beam sonar to map seagrass beds in Otsuchi Bay on the Sanriku Coast of Japan. *Aquat. Living Resour.* **2003**, *16*, 223–230. [[CrossRef](#)]
102. Lee, K.M.; Ballard, M.S.; McNeese, A.R.; Wilson, P.S. Sound speed and attenuation measurements within a seagrass meadow from the water column into the seabed. *J. Acoust. Soc. Am.* **2017**, *141*, EL402–EL406. [[CrossRef](#)]
103. Zecchin, M.; Baradello, L.; Brancolini, G.; Donda, F.; Rizzetto, F.; Tosi, L. Sequence stratigraphy based on high-resolution seismic profiles in the late Pleistocene and Holocene deposits of the Venice area. *Mar. Geol.* **2008**, *253*, 185–198. [[CrossRef](#)]
104. Zecchin, M.; Brancolini, G.; Tosi, L.; Rizzetto, F.; Caffau, M.; Baradello, L. Anatomy of the Holocene succession of the southern Venice lagoon revealed by very high-resolution seismic data. *Cont. Shelf Res.* **2009**, *29*, 1343–1359. [[CrossRef](#)]

